THE JOURNAL OF PHYSICAL CHEMISTRY A

Article

pubs.acs.org/JPCA

Peierls Stress of Dislocations in Molecular Crystal Cyclotrimethylene Trinitramine

Nithin Mathew,[†] Catalin R. Picu,*[,†] and Peter. W. Chung[‡]

[†]Department of Mechanical, Aerospace and Nuclear Engineering, Rensselaer Polytechnic Institute, Troy, New York 12180, United States

[‡]Weapons and Materials Research Directorate, U.S. Army Research Laboratory, Aberdeen Proving Ground, Maryland 21005-5066, United States

ABSTRACT: Dislocation mediated plasticity in the α phase of the energetic molecular crystal cyclotrimethylene trinitramine (RDX) was investigated using a combination of atomistic simulations and the Peierls−Nabarro (PN) model. A detailed investigation of core structures and dislocation Peierls stress was conducted using athermal atomistic simulations at atmospheric pressure to determine the active slip systems. Generalized stacking fault energy surfaces calculated using atomistic simulations were used in the PN model to also estimate the critical shear stress for dislocation motion. The primary slip plane is found to be (010) in agreement with experimental observations, with the (010)[100] slip systems having the lowest Peierls stress. In addition, atomistic simulations predict the (021)[0$\bar{1}$2], (021)[100], (011)[100], (001)[100], and (001)[010] slip systems to have Peierls stress values small enough to allow plastic activity. However, there are less than five independent slip systems in this material in all situations. The ranking of slip systems based on the Peierls stress values is provided, and implications are discussed in relation to experimental data from nanoindentation and shock-induced plastic deformation.

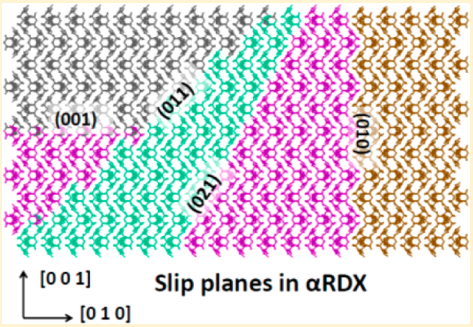

1. INTRODUCTION

Cyclotrimethylene trinitramine (RDX), an energetic molecular crystal, is used in many explosive formulations for both civilian and military purposes. Initiation and detonation in explosives is considered to happen by formation of regions of localized energy called "hot spots." Theoretical considerations[1] have proposed that hot spots need to have micrometer dimensions and sustain high temperatures (~500 °C) for microseconds. Various theories have been proposed regarding the precise mechanisms of hot-spot formation. In polymer bonded explosives, local heterogeneity, presence of defects (dislocations, pores, cracks), and/or adiabatic heating due to plastic deformation are thought to contribute toward formation of hot spots. Experimental and theoretical studies in single crystals have suggested different mechanisms. Dislocation pileup and subsequent energy release on depinning have been proposed[2] as a mechanism for hot-spot formation in single crystals. Anisotropic activation of slip systems was found to correlate with the observed anisotropic response of shock-loaded pentaerythritol tetranitrate single crystals, and this led to the development of the steric hindrance model.[3] According to this model, the lack of activated slip systems for a particular crystallographic orientation leads to deformation of molecules, resulting in bond breaking and subsequent release of energy which eventually produces initiation.

Owing to their suspected role in processes leading to detonation, plastic deformation mechanisms operating in RDX have been investigated by computational and experimental means. Dynamic yield points determined from shock loading of single crystals at a Rankine−Hugoniot pressure (P_{RH}) of 2.25 GPa for (111), (021), and (100) planes were reported to be isotropic.[4] The response, described in terms of the shape of the velocity history profiles, was found to exhibit significant variation depending on the shock direction. Plate impact experiments in the (111) direction[5] indicated a change in response as the pressure varied from 1.25 to 2.25 GPa. This variation was attributed to the nucleation of (001)[010] partials upon shock loading and subsequent plastic hardening, which was validated using molecular dynamics simulations. The observation was also used to explain the anomalous response of (021) shocked RDX crystals.[6] High pressure (7−20 GPa) plate impact experiments on the (111), (210), and (100) planes[7] revealed considerable anisotropy in shock decomposition of RDX. Crystals shocked perpendicular to the (210) and (100) planes were found to be more sensitive compared to those shocked perpendicular to the (111) plane. In the present study we propose an interpretation of this observation based on the mechanisms of dislocation-mediated plasticity.

X-ray diffraction, microindentation, and etch-pitting were used to correlate deformation features with possible active slip systems in RDX. Experimental studies from different sources have proposed (010) as the primary slip plane.[8,9] Micro-

Received: February 6, 2013
Revised: June 2, 2013
Published: June 4, 2013

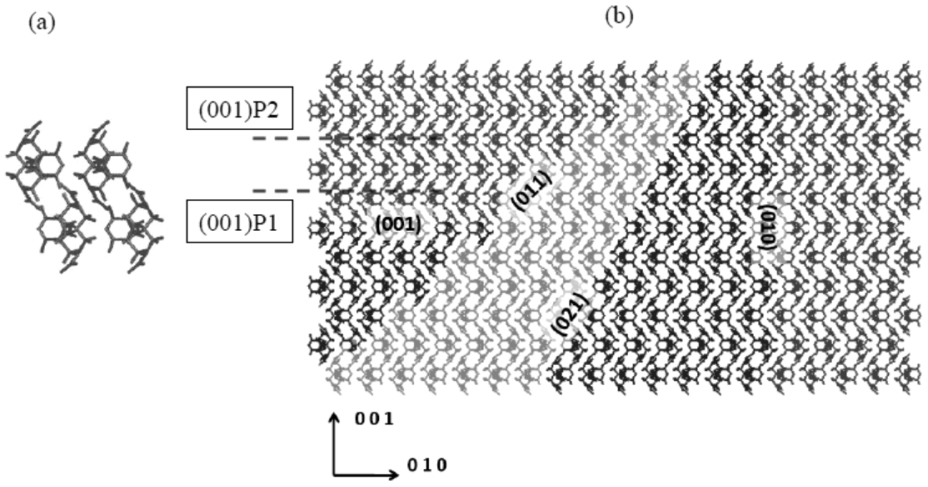

Figure 1. (a) Unit cell of α-RDX in the [100] projection. (b) α-RDX crystal in the (100) projection with the slip planes considered in this study shown. The two types of slip plane (P1 and P2) are indicated for (001).

indentation studies by Gallagher et al.[10] suggested slip systems of the {021}[100] and (010)[001] type. Investigations by Halfpenny et al.[11] also suggest (010) as the primary slip plane and hinted at the possibility that {011} or {021} could be secondary slip planes. Nanoindentation experiments performed on (210), (021), and (001) oriented crystals of RDX showed elastic−plastic load excursion at estimated resolved shear stresses within the $G/15$ to $G/10$ range,[12] where G is the shear modulus. These observations were attributed to the homogeneous nucleation of dislocations. The hardness values were reported to be nearly isotropic, but significant variation was observed for the load at the first "pop-in" event. Tomography of indent impressions revealed features consistent with slip on (010), {021}, and {011} planes, and it was conjectured that RDX exhibits hindered plasticity due to the lack of independent slip systems. Munday et al.[13] investigated the competition between ductile deformation and brittle fracture using generalized stacking fault surfaces coupled with Rice's criterion for dislocation emission from the crack tip.[14] They found that the (010), (011), (021), and (001) planes possess slip systems exhibiting ductile behavior.

A consensus exists in the literature regarding slip on the (010), {021}, and {011} planes.[8,9,11−13] Recent molecular dynamics simulations have also indicated possible slip on (001) planes.[5,13] Activation of slip systems requires that the resolved shear stress is higher than the critical stress (Peierls stress) required for the motion of individual dislocations on the respective slip system. Knowledge of Peierls stresses is essential in understanding preferential activation of slip systems under a general state of stress.

In this study, fully atomistic simulations are performed to evaluate this critical stress. The investigation was conducted for the (010), (001), (011), and (021) crystallographic planes in α-RDX, which are shown in Figure 1. As discussed above, these planes are expected to display ductile behavior. The [100] slip direction in all the above planes is studied, which has been proposed[12,13,15] as a possible cross-slip direction. In addition, the (010)[001], (001)[010], (021)[$0\bar{1}2$], and (011)[$0\bar{1}1$] systems are considered, which have been also suggested in the literature as possible slip systems.[13,15]

2. METHODOLOGY

α-RDX is modeled using the flexible Smith−Bharadwaj potential developed for condensed phase nitramines.[16] The potential has been reported to accurately reproduce elastic and thermal properties of RDX.[5] Nonbonded interactions, which includes electrostatic and van der Waals interactions, are explicitly considered up to a cutoff radius of 10 Å.The charges are modified to account for the effects of polarization in the condensed phases.[16] Bonded interactions are represented with angle-bending, bond-stretching, and dihedral interactions. Compared with the other potential available for RDX, the Sorescu−Rice−Thompson potential,[17] which represents the molecules as rigid entities, the Smith−Bharadwaj potential allows molecular flexibility. As discussed in this paper, molecular conformation changes are important in the mechanics of crystal defects. This has determined the choice of force field in this work. A schematic of the simulation setup is shown in Figure 2. For the (010) and (001) planes, the simulation cell is of size 100 × 2 × 100 unit cells respectively in the **n**, **p**, and **q** directions and consists of 3 360 000 atoms. The simulation cell size was selected as large as possible in order to

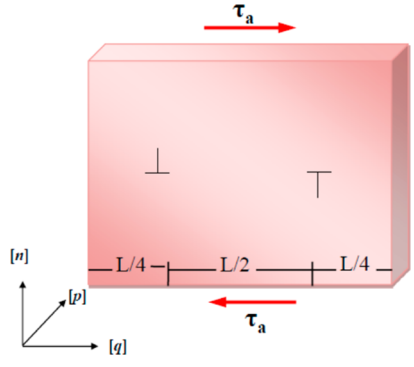

Figure 2. Simulation setup. In the figure, **p**, **q**, and **n** form an orthogonal coordinate system. In all simulations, the glide plane normal (**g**) is aligned with **n**. For edge dislocation dipoles, the dislocation line direction ($\boldsymbol{\xi}$) is aligned with **p** and the Burgers vector (**b**) is aligned with **q**. For screw dislocation dipoles, $\boldsymbol{\xi}$ and **b** are aligned along **p**. τ_a represents the applied shear stress in the **b** direction and is shown in the figure as applied to an edge dislocation dipole. L denotes the length of the simulation cell.

dx.doi.org/10.1021/jp401368t | J. Phys. Chem. A 2013, 117, 5326−5334

reduce the effect of the boundary conditions on the quantities of interest, while staying within our current computational capabilities. In all simulations, the glide plane normal (**g**) is aligned with **n**. For edge dislocation dipoles, the dislocation line direction ($\boldsymbol{\xi}$) is aligned with **p** and the Burgers vector (**b**) is aligned with **q**. For screw dislocation dipoles, $\boldsymbol{\xi}$ and **b** are aligned with **p**. Long-range interactions are calculated using the particle-particle-particle-mesh (PPPM) algorithm.

For the (011) and (021) planes, periodicity in the glide plane requires use of nonorthogonal simulation cells. For simulations on these slip planes, the simulation cell were of sizes 30 × 2 × 50 and 20 × 2 × 32, respectively, in the **n**, **p**, and **q** directions. The Ewald/*N* algorithm was used to calculate long-range interactions in simulations with nonorthogonal cells. In all cases, a vacuum pad is included in the direction perpendicular to the glide plane. Both orthogonal and nonorthogonal cells are shown in Figure 3.

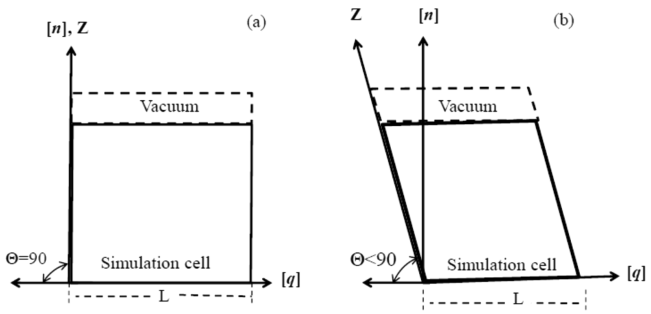

Figure 3. Schematic of the simulation cells used in the study. **Z** represents the simulation box vector used to define the periodicity. **n**, **q**, and *L* are defined in Figure 2. (a) Orthogonal cells were used for the (010) and (001) slip planes. (b) Nonorthogonal cells were used for the (011) and (021) slip planes.

α-RDX has an orthorhombic structure with the space group *Pbca*. There are eight molecules per unit cell, with all molecules in the Caae conformation. The conformational state of RDX molecule is defined by the shape of the ring (chair denoted by "C", boat denoted by "B", or twist denoted by "T") and the position of the three nitro groups (axial denoted by "a" and equatorial denoted by "e"). A nitro group oriented in the direction parallel to the ring normal is considered axial.

The initial structure was created using neutron-diffraction data from Choi and Prince[19] and was allowed to relax at 0 K and atmospheric pressure. A dislocation dipole was created by imposing the Volterra displacement field on the centers of mass (COM) of the molecules, which ensures that the molecular bonds and angles are not distorted by the applied displacement field. The individual dislocations of the dipole are arranged on the same glide plane in such a way that a periodic array of dipoles results (on the glide plane) upon application of periodic boundary conditions. The distances between the dislocations in the unit cell and that between these and their images are equal. This ensures that the Peach–Koehler force acting on each dislocation due to the interaction with others in the periodic array vanishes in the initial, unloaded configuration. This holds in materials with generic anisotropy since the resolved shear stress in the direction of the Burgers vector and in the glide plane is always symmetric relative to the position of the core.[18] An image exists in the direction of the vacuum pads, but no infinite array of images exists in the **n** direction. When the model is distorted and the dislocation cores shift, the interaction with images in the glide plane produces a net Peach–Koehler force on each dislocation of the dipole. This introduces a small error in the estimation of the Peierls stress. This error was estimated using the linear elastic solution, based on the shift of the cores by **b**/2, i.e., a shift corresponding to the peak of the Peierls barrier, and was found to be less than 1% in all cases considered.

It should also be noted that, since each molecule remains electrically neutral during deformation, the cores do not carry electric charges. Electric dipoles may exist due to the large deformations, but their field decays faster than the elastic field; hence the dipole–dipole interaction of the cores with their images is weak.

An infinitely long (and straight) dislocation is created upon application of periodic boundary conditions in the **p** direction. A resolved shear stress (τ) is imposed so that the individual dislocations of each dipole move toward each other, i.e., toward the center of the simulation cell. This is done by applying a homogeneous shear strain to all COM of molecules in the relaxed model, followed by relaxation while holding the boundaries of the model fixed. The boundary is maintained fixed by zeroing the forces in all directions on a layer of two unit cell thickness at the boundary. The presence of the vacuum pads in the **n** direction facilitates the application of this distortion. To prevent significant steric hindrance due to the rigid shift of the molecules in this step, the relaxation is divided in two stages. In the first stage a repulsive potential is added to the nonbonded interactions to help separate the potentially overlapping molecules and few relaxation steps are taken. Then, this dummy field is removed and relaxation proceeds normally. In addition, the displacement imposed in each loading step is kept small to reduce the likelihood of overlaps.

The applied shear strain was increased, starting each time with the relaxed stress-free dislocation structure, until the dislocation was found to shift by at least one lattice spacing. The corresponding stress value is the Peierls–Nabarro stress (τ_{PN}) of an infinitely long, straight dislocation of the particular type. For partials, the Peierls–Nabarro stress is calculated as the sum of the critical stress and the contribution to the Peach–Koehler force from the stacking fault. When considering partials, the stacking fault is always located between the two dislocations explicitly represented in the model; hence its action is to pull them toward each other. The stacking fault energy was obtained from the literature.[13]

All simulations were performed using LAMMPS, a molecular simulation code from Sandia National Laboratories.[20] Minimizations were performed using the conjugate gradient algorithm. Residual kinetic energy was drained by running damped dynamics with a damping constant of 20 kcal/mol·fs until the temperature of the simulation cell was below 0.2 K. Simulations were performed using 1024 processors on the Blue-Gene/L at the Computational Center for Nanotechnology Innovations (CCNI) at Rensselaer Polytechnic Institute.

3. RESULTS

3.1. Structure of Dislocation Cores. The core structure is evaluated by calculating the relative displacement of the COM of molecules across the glide planes ($u(x)$).The width of the dislocation, *w*, is defined as the distance between the two inflection points of $u(x)$, i.e., approximately $b/4 \leq u(x) \leq 3b/4$. A wide, planar core would be easier to move than a compact core. The equation $u(x) = b \arctan[(x - x_0)/w]$ is fitted to the

dx.doi.org/10.1021/jp401368t | J. Phys. Chem. A 2013, 117, 5326–5334

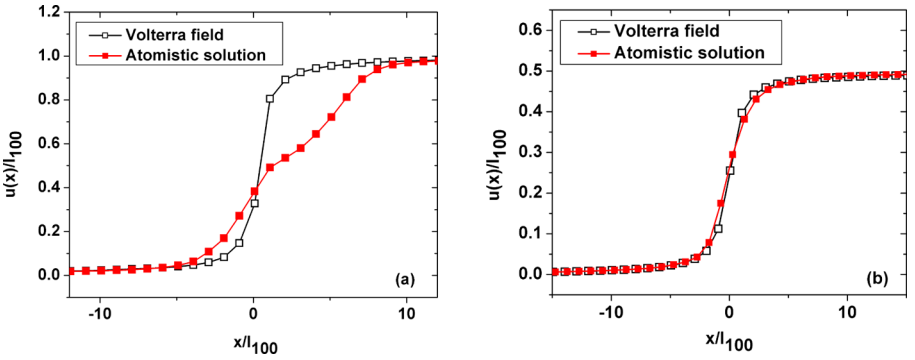

Figure 4. Structure of the (010)[100] edge dislocation. (a) The dislocation with **b** = [100] splits into two partials of **b** = 1/2[100]. (b) Structure of the **b** = 1/2[100] partial.

core profiles of stable dislocations resulting from the simulation in order to evaluate the widths.

Dislocations are considered to be stable if, upon minimization, the molecular layers on either side of the glide plane did not separate (cleave) and the magnitude of the Burgers vector remained equal to that corresponding to the applied displacement field. The various slip planes considered in the study are schematically represented in Figure 1, and the core structures obtained from atomistic calculations are presented in this section. For each crystallographic plane there exist two parallel slip planes which differ in the nature of intermolecular bonding across the glide plane. An example is shown in Figure 1, where it is apparent that two different types of (001) planes form the stacking, with two others in the sequence being identical, but rotated by 180° relative to the [001] axis. The planes differ in attachment (cohesive) energies as described previously.[13] In the present study only the planes with lower cohesive energies are considered.

3.1.1. (010) Plane. Two directions of the Burgers vector are considered in the (010) plane: the [100] and the [001]. In each case the screw and edge dislocations are studied. The (010)[100] slip system has been reported in previous studies to exhibit dislocation activity.[12,13] Slip was also reported in the (010)[001] system in previous experimental investigations.[8,10] The [100] direction was reported[13] to have a stable stacking fault at **b** = 1/2[100] with a stacking fault energy of 101 mJ/m^2.

Let us consider first the edge dislocation. It was found in our simulations that the edge dislocations of the (010)[100] type with **b** = [100] are not stable and dissociate into partials of pure edge character with **b** = 1/2[100], therefore providing support to the observation of a minimum in the [100] trace of the γ-surface at a relative shift of 1/2[100]. The structure of the relaxed core is compared to the structure of the Volterra dislocation[21] in Figure 4a. Figure 4b shows the structure of a **b** = 1/2[100] partial dislocation. The split of the dislocation with **b** = [100] in two partials is clearly observed in Figure 4a, while the partial dislocation with **b** = 1/2[100] has a compact core, very close to that of the Volterra dislocation.

Full screw dislocations of the (010)[100] type were stable when τ = 0, but were found to split into partials with **b** = 1/2[100] when a resolved shear stress of at least 0.2 GPa was applied. Therefore, the core with full Burgers vector, **b** = [100], is lattice trapped and is essentially unstable. The resolved stress applied to assist the split of the dislocation into partials is close to the resolved stress required to move the **b** = 1/2[100] partial. This perturbation helps the system to reduce its energy into a configuration compatible with the minimum of the γ-surface mentioned above. Dislocations of the (010)[001] type did not split and relaxed to narrow core structures with **b** = [001]. The calculated widths of all stable configurations are reported in Table 1.

Table 1. Ranking of Slip Systems Resulting from the Atomistic Models

slip plane	type	τ_a (GPa)	ϵ_{τ_a} (GPa)	τ_{SF} (GPa)	τ_{PN} (GPa)	w (Å)
(010)	1/2[100]/edge	0.050	0.012	0.151	0.201	29.48
(010)	1/2[100]/screw	0.129	0.034	0.151	0.280	21.68
(001)	[010]/screw	0.458	0.044	0.000	0.458	17.08
(001)	1/2[100]/screw	0.170	0.012	0.308	0.478	20.29
(021)	1/2[0$\bar{1}$2]/screw	0.356	0.039	0.142	0.498	10.20
(011)	[100]/screw	0.518	0.064	0.000	0.518	14.11
(021)	[100]/screw	0.524	0.037	0.000	0.524	8.85
(021)	1/2[100]/edge	0.296	0.037	0.280	0.576	16.95
(011)	[100]/edge	0.583	0.064	0.000	0.583	20.25
(001)	1/2[100]/edge	0.287	0.048	0.308	0.595	36.89
(021)	[0$\bar{1}$2]/screw	0.635	0.039	0.000	0.635	8.33
(001)	1/2[010]/edge	0.240	0.044	0.406	0.646	30.07
(021)	1/2[100]/screw	0.382	0.037	0.280	0.662	14.94
(010)	[001]/edge	0.782	0.059	0.000	0.782	12.77
(010)	[001]/screw	0.831	0.059	0.000	0.831	14.77
(011)	[0$\bar{1}$1]/screw	0.896	0.075	0.000	0.896	6.51

3.1.2. (001) Plane. Experimental studies[8] have suggested the (001) plane to be a cleavage plane in RDX. Molecular dynamics simulations of shocked RDX crystals[5] reported nucleation of 0.16[010] partials on the (001) planes. Ductile behavior was reported for both the (001)[100] and (001)[010] slip systems in ref 13 with stable stacking faults at **b** = 1/2[100] and **b** = 1/2[010]. The [010] and [100] directions in this plane are investigated in this study.

Edge and screw dislocations with **b** = [100] split into partials of 1/2[100] type upon the application of a resolved shear stresses of at least 0.4 GPa. This lattice trapping effect is similar to that discussed for the (010) plane. The width of (001)[100] dislocations are reported in Table 1.

Only screw type full dislocations with **b** = [010] were stable. Edge dislocations with the same Burgers vector were unstable

dx.doi.org/10.1021/jp401368t | J. Phys. Chem. A 2013, 117, 5326−5334

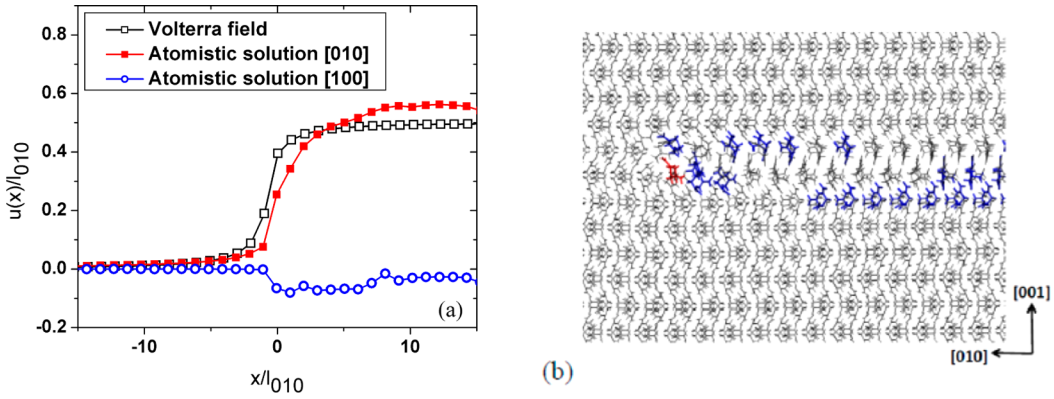

Figure 5. Core structure of the (001)[010] edge dislocation with **b** = 1/2[010]. (a) Relative displacement of COM across the glide plane. (b) Molecular conformational state of the core in (a). Caaa molecules are colored in red, Caee are in blue, and Caae are in gray.

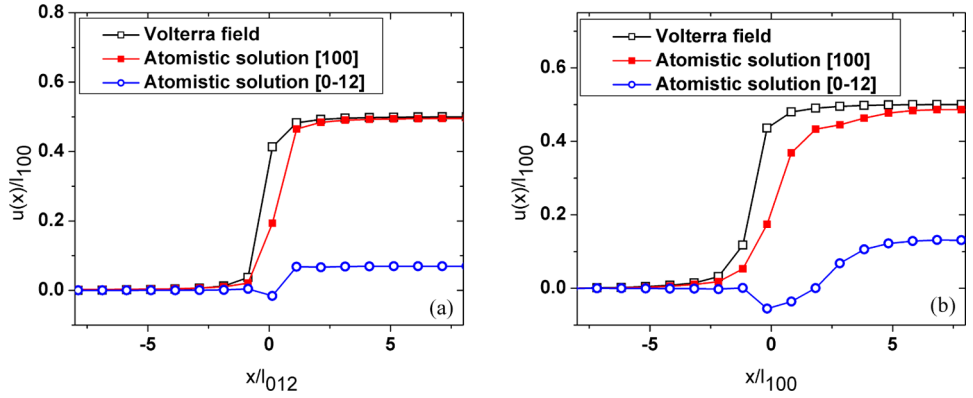

Figure 6. Core structure of **b** = 1/2 [100] dislocations residing on the (021) plane. (a) Screw dislocation. (b) Edge dislocation.

and only partials with **b** = 1/2[010] could be stabilized. The core structures of the (001)1/2[010] edge dislocations are shown in Figure 5a. For these partials, rotation and conformational flips (Caae to Caee) of the molecules across the glide plane are observed and an out-of-plane component with **b** = 0.1[100] develops.

The atomistic core structure of the edge partial is shown in Figure 5b. Conformation changes of the molecules are observed in the core and in the region of the stacking fault. The molecules colored in blue are in the Caee state, those in red are in the Caaa state, and all others are in the Caae ground state. Most molecules in the stacking fault are in the Caae conformation, but are rotated relative to the molecules in the perfect crystal. Different packing is observed in the stacking fault region. It should be also noted that the rotation of the molecules leads to a shift of the COM which reflects in the $u(x)$ profiles shown in Figure 5a. The apparent out-of-plane component, $u_{[100]}(x)$, as well as the deviation of the $u_{[010]}(x)$ trace from the Volterra solution in the stacking fault region (right side of the plot) are due to this COM shift and do not represent physical dislocation components or a real variation of the Burgers vector length.

3.1.3. (021) Plane. The (021) plane contains the slip systems (021)[100] and (021)[0$\bar{1}$2]. Edge and screw dislocations with **b** = [100] and **b** = 1/2[100] were found to be stable. This agrees with the presence of a minimum in the γ-surface reported for the (021)[100] system at the 1/2[100] position.[13] Upon application of a resolved shear stress of 0.55 GPa, an edge dislocation with the full Burgers vector, **b** = [100], was found to lead to cleavage starting from the core, which indicates that the lattice trapping is too strong in this direction to let the core relax and split into partials. The screw dislocation with **b** = [100] does not lead to cleavage but is also incapable of relaxation by splitting into partials. The partials with **b** = 1/2[100] are stable in both the edge and screw configurations, and their core profiles are shown in Figure 6. As with the (001)[010] partial of Figure 5, apparent out-of-plane components of **b** = 0.1[0$\bar{1}$2] type are observed upon relaxation; these are due to COM shifts associated with molecular conformation changes in the core. Screw dislocations with **b** = [0$\bar{1}$2] and **b** = 1/2[0$\bar{1}$2] were found to be stable, and the calculated widths are reported in Table 1.

3.1.4. (011) Plane. The [100] and [0$\bar{1}$1] directions are considered in this plane. The possibility of cross-slip in the [100] direction was postulated in previous studies.[12,13] The (011)[0$\bar{1}$1] slip system was reported to exhibit brittle response. A stable stacking fault at **b** = 1/2[100] was reported in ref 13 but was not reproduced in our atomistic simulations. The widths of stable dislocations with full Burgers vector on the (011)[100] and (011)[0$\bar{1}$1] slip systems are reported in Table 1.

3.2. Ranking of Slip Systems. *3.2.1. Peierls Stress from Atomistic Simulations.* The stable dislocations are ranked in Table 1 in the order of increasing τ_{PN}. Table 1 also includes the critical stress applied in the simulation (τ_a) which puts the dislocation in motion, the contribution from the stacking fault energy (τ_{SF}) to the Peach–Koehler force, and the width (w) calculated by fitting the relaxed core structure, as described in section 3.1.The contribution of the stacking fault to the critical stress is calculated as

dx.doi.org/10.1021/jp401368t | J. Phys. Chem. A 2013, 117, 5326−5334

$$\tau_{SF} = \frac{\gamma_{SF}}{b} \quad (1)$$

where γ_{SF} is the stable stacking fault energy and b is the magnitude of the Burgers vector. The Peierls stress is calculated as

$$\tau_{PN} = \tau_a + \tau_{SF} \quad (2)$$

indicating the fact that the stacking fault aids the motion of partials in all models considered. The error in τ_a, ϵ_{τ_a}, is the range in which the Peierls stress is observed. Specifically, the dislocation moves at the stress denoted as τ_a, but it does not move at $\tau_a - \epsilon_{\tau_a}$.

The Peierls stresses for stable dislocations are shown in Figure 7 as a function of the theoretical strength. The bars in Figure 7 represent ϵ_{τ_a}. The theoretical strength is calculated using the formula[21]

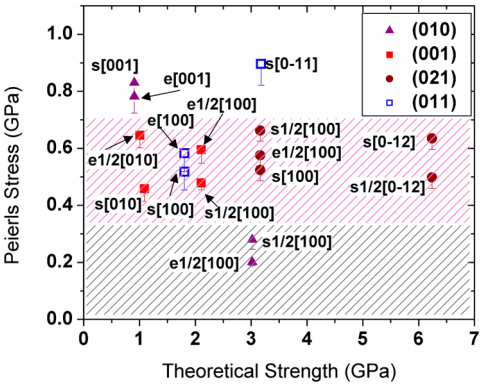

Figure 7. Peierls stress values evaluated in atomistic simulations versus the theoretical strength in the respective crystal direction. The "e" and "s" labels stand for edge and screw dislocations, respectively. The bars represent the range in which the Peierls stress is observed. The limits defining the two shaded areas are selected arbitrarily to correspond to $G_v/20$ and $G_v/10$, where G_v is the Voigt shear modulus, eq 4. $G_v/10$ is close to the theoretical shear strength of the crystal.

$$\tau_{TS} = (a/d)\frac{G}{2\pi} \quad (3)$$

Here G represents the shear modulus in the appropriate crystallographic direction, a is the intermolecular spacing in the **b** direction, and d is the interplanar spacing for the respective glide plane. One observes a clear demarcation in the distribution of the Peierls stress values close to 350 MPa. This value is close to $G_v/20$, where G_v is the Voigt average shear modulus, calculated as[22]

$$G_v = \frac{1}{15}(C_{11} + C_{22} + C_{33} - C_{23} - C_{13} - C_{12}) + \frac{1}{5}(C_{44} + C_{55} + C_{66}) \quad (4)$$

Here C_{ii} are the components of the stiffness matrix. The calculated value of G_v at 0 K using the moduli reproduced by this potential is equal to 7.004 GPa, and the τ_{PN} values are discussed here in terms of the fraction of G_v.

Dislocations on the (010)[100] slip system have the lowest Peierls stress ($\tau_{PN} < G_v/20$). Thus the (010) plane is found to be the primary slip plane, in agreement with multiple experimental observations. For slip systems of the type (021)[0$\bar{1}$2], (021)[100], (011)[100], (001)[010], and (001)[100], the simulations yield $G_v/20 < \tau_{PN} < G_v/10$. The third regime consists of slip systems of the type (011)[0$\bar{1}$1] and (010)[001], with $\tau_{PN} > G_v/10$. Out of the slip systems in the third regime, (010)[001] systems can be considered inactive, since the critical stresses calculated are close to the theoretical strength and cleavage is likely to happen before plastic deformation. This result is not in agreement with previous suggestions made based on indirect experimental observations.[8,12]

It is noted here that screw dislocations of the [100] type on the (021), (001), and (011) planes have critical stress values of 0.524, 0.478, and 0.518 GPa, thus indicating the possibility of cross-slip between these planes, in situations where the resolved stresses are higher than 0.524 GPa. Cross-slip has been suggested between planes containing the common [100] slip direction in other studies.[12,13,15] The present results confirm that this is possible from the point of view of the lattice resistance to slip. The unstable stacking fault energies for these slip systems reported in the literature[13] are also within a narrow range of each other. The critical stress for the [100] screw dislocation on the (010) plane is 0.28 GPa, which is much lower than the values for the other planes.

3.2.2. Peierls Stress Calculations Using the Peierls–Nabarro Model. The Peierls–Nabarro (PN) model is based on an interpretation of the core of a dislocation as a continuous distribution of infinitesimal dislocations on the glide plane. The relevant parameter describing the core shape becomes the density of these infinitesimal dislocations, $\rho = \partial u/\partial x$. The model requires the equilibrium of the distribution, which is written in terms of the force resulting from the elastic interaction of the infinitesimal dislocations, the lattice rebound force, and the applied far-field resolved shear stress. All PN models assume that the core is planar. The equilibrium condition is written as

$$\frac{G'}{2\pi}\int_{-\infty}^{\infty}\frac{1}{x - x'}\frac{d(u(x'))}{dx'}dx' = F_\gamma(u(x)) + \tau \quad (5)$$

where

$$G' = G\left(\frac{\sin^2\theta}{1-\nu} + \cos^2\theta\right) \quad \text{and} \quad F_\gamma = -\frac{d\gamma(u)}{du} \quad (6)$$

Here $G'/2\pi$ is the energy prefactor, θ is the angle between vectors **b** and **ξ**, G is the isotropic shear modulus, ν is the Poisson's ratio, F_γ is the lattice restoring force obtained as the derivative of the γ-surface trace in the direction of **b**, and τ is the applied resolved shear stress. A normalization condition is required, which is written as

$$\int_{-\infty}^{\infty}\frac{d(u(x'))}{dx'}dx' = b \quad (7)$$

The equilibrium core structure, $u(x)$, is obtained by solving eq 5 without the applied shear stress. The unknown function $u(x)$ is written as a superposition of arctan functions as

$$u(x) = \frac{b}{\pi}\sum_{i=1}^{4}\alpha_i \arctan\left(\frac{x - x_i}{c_i}\right) + \frac{b}{2} \quad (8)$$

The Peierls stress can be obtained by increasing the value of τ until no solutions are found for eq 5. This value of τ is the critical stress required to move the dislocation on the glide plane (τ_{PN}^{γ}). Note that this version of the PN model provides

dx.doi.org/10.1021/jp401368t | J. Phys. Chem. A 2013, 117, 5326–5334

only an approximation of the dislocation core since it does not include nonlocal effects and out-of-plane displacements (shear−tension coupling). If the relative motion of the crystal planes involves dynamic changes of the conformation state of the molecules, the PN model cannot account for this physics even when the restoring force is computed from the γ-surface evaluated from atomistic models (eq 6).

γ-surfaces for the slip systems considered in this study have been published elsewhere.[13] The Peierls stress values obtained from the PN model (τ_{PN}^{γ}) are compared with the values obtained from atomistic simulations in Figure 8.

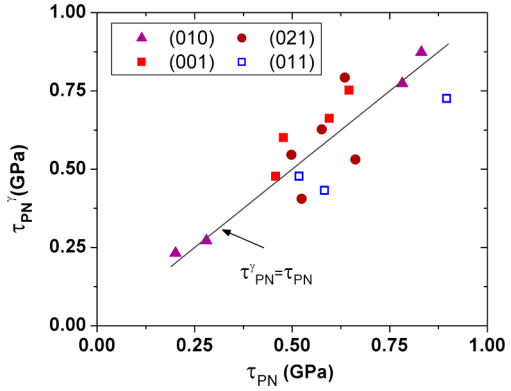

Figure 8. Comparison between Peierls stress values obtained from the PN model (τ_{PN}^{γ}) and atomistic simulations (τ_{PN}).

The (010)[100] system is found to be the most easily activated system with $\tau_{PN}^{\gamma} < G_v/20$ in agreement with the predictions obtained from atomistic simulations. Slip systems of the types (010)[001] and (011)[0$\bar{1}$1] and edge dislocations with **b** = 1/2[010] on (001) planes were found to have $\tau_{PN}^{\gamma} > G_v/10$. The values obtained from the PN model for all slip systems are within 20% of the atomistic results, except for the (021)[0$\bar{1}$2], (011)[100], and (001)[100] slip systems for which the error is about 25%. This provides support for the use of the PN model when estimating Peierls stresses. The computational effort associated with estimating the γ-surface and solving the PN model for a particular slip system is much smaller than that required to determine the Peierls stress from full atomistic simulations, since very large atomistic models are required in the latter case.

4. DISCUSSION

The atomistic results can be analyzed from a classical continuum perspective. Compatibility conditions require that five independent slip systems are required in a crystal to accommodate an arbitrary applied strain. This constraint is relaxed in complex ways near surfaces. The ability of the RDX crystal to accommodate an arbitrary plastic strain can be investigated using the method proposed by Kocks[23] and Kelly and Groves[24] for low symmetry crystal structures. This method was recently employed for RDX using information resulting indirectly from nanoindentation experiments.[12] The strains produced by unit slip on all slip systems considered in this study are shown in Table 2.

Assuming that all eight slip systems considered are activated, one can form a total of 56 ($^8C_5$) unique combinations of possible groups of five slip systems. Though this is the case, none of these 56 groups possess the required five independent slip systems. At the most, one obtains four independent systems and this points to the fact that plasticity in RDX is hindered even when all eight slip systems investigated are active.

Additional considerations come into play when the ranking of slip systems presented in Table 1 is taken into account. Recent nanoindentation experiments[12] performed on RDX reported first pop-in events at 246, 368, and 994 μN applied indentation force for indents in the (210), (021), and (001) faces, respectively. A simple analysis based on Schmid factors shows that, without taking into account the Peierls stress, five, three, and two slip systems could be activated for the (210), (021), and (001) cases, respectively. Let us consider the point located at 0.48a, with a being the contact radius of the indenter, below the surface and on the symmetry axis. In an isotropic material, this is the point where the maximum shear stress is reached and is also the point where homogeneous dislocation nucleation is usually assumed to take place. We compute the resolved shear stress in all slip systems studied with the goal of estimating the number of systems in which activity may take place at the critical indentation loads observed in experiments. These resolved shear stresses are plotted against the lowest values of τ_{PN} for the respective slip systems in Figure 9.

For indentation on the (210) face, activity is enabled on the (010)[100] system, for indentation on the (021) plane only screw dislocations on (001)[010] can move, and indentation on the (001) face leads to the activation of (021)[0$\bar{1}$2] at the load corresponding to the first pop-in event. This indicates that at the first plastic event only one slip system is activated in all situations. This is meaningful since one expects that the first sign of plasticity under the indenter may be produced by activity on one slip system only. However, the critical loads predicted using our data would underestimate the loads observed in experiments. Specifically, the (010)[100] system is activated when the applied force normal to the (210) face is 12 μN, the (001)[010] system would operate at a force normal to the (021) face of 208 μN, and the (011)[0$\bar{1}$1] system becomes active at a critical load perpendicular to the (001) face

Table 2. Components of Strain Resulting from Unit Slip on Specific Slip Systems

slip system	slip plane normal	slip vector	ε_{11}	ε_{22}	ε_{33}	$2\varepsilon_{23}$	$2\varepsilon_{31}$	$2\varepsilon_{12}$
(010)[100]	[0 1 0]	[1 0 0]	0	0	0	0	0	1
(010)[001]	[0 1 0]	[0 0 1]	0	0	0	1	0	0
(001)[100]	[0 0 1]	[1 0 0]	0	0	0	0	1	0
(001)[010]	[0 0 1]	[0 1 0]	0	0	0	1	0	0
(021)[100]	[0 0.877 0.481]	[1 0 0]	0	0	0	0	0.481	0.877
(021)[0$\bar{1}$2]	[0 0.877 0.481]	[0 −0.481 0.877]	0	−0.422	0.422	0.538	0	0
(011)[100]	[0 0.674 0.739]	[1 0 0]	0	0	0	0	0.739	0.674
(011)[0$\bar{1}$1]	[0 0.674 0.739]	[0 −0.739 0.674]	0	−0.498	0.498	−0.092	0	0

dx.doi.org/10.1021/jp401368t | J. Phys. Chem. A 2013, 117, 5326−5334

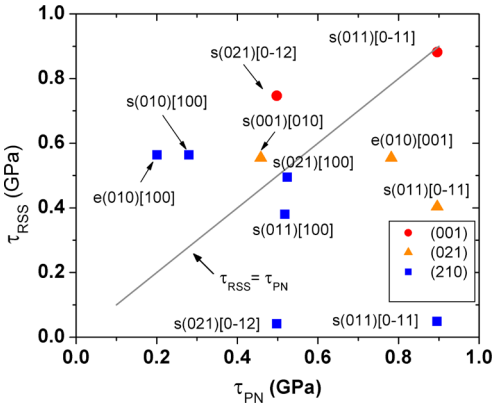

Figure 9. Activation of slip systems in indentation experiments perpendicular to the (001), (021), and (210) crystal planes.[12] "e" and "s" stand for edge and screw dislocations, respectively.

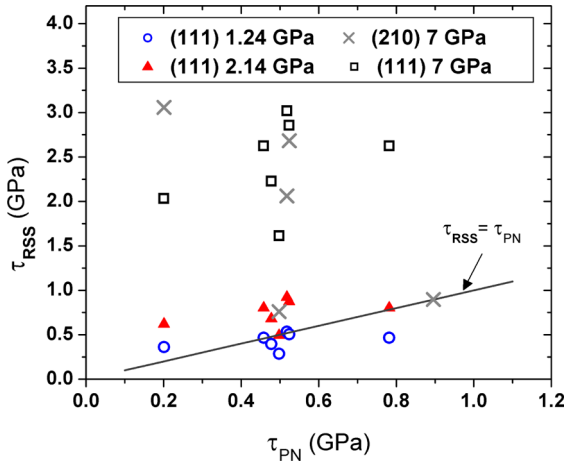

Figure 10. Activation of slip systems for (111) and (210) shocks.

of 295 μN. The present analysis predicts the proper anisotropy of the indentation response, with the (210) indents having the lowest critical load and the (001) indents having the highest one. The underestimation is also expected. If the pop-in event is produced by dislocations that nucleate homogeneously under the indenter, the load required for nucleation should be much larger than that required for motion of an existing dislocation since the respective energetic barriers are quite different. Likewise, if the pop-in event is due to preexisting dislocations, the critical load should not only put these dislocations in motion, but should also be large enough to render unstable the preexisting dislocation structures. Therefore, in both situations, the first pop-in loads predicted based on the Peierls stress values are expected to be smaller than those observed experimentally. Since the mechanism leading to the first pop-in is not entirely known, the observation made here that the ranking of the activated slip systems in terms of Peierls stresses matches the experimental anisotropy in indentation should not be overemphasized. We interpret it as a suggestion that, since Peierls stresses are very large in these crystals, the critical stress required to put dislocations in motion should be close to the critical stress of the mechanism leading to criticality in indentation.

Let us consider the implications of the results presented in this article in the context of anisotropic sensitivity of RDX shocked perpendicular to the (111), (210), and (100) planes. Calculation of Schmid factors shows[7] that (111) shocks could activate seven slip systems, (210) shocks provide nonzero resolved shear stress on five slip systems, and (100) shocks do not activate any slip system, even when the (001) systems are taken into consideration. (111) shocks activate systems (001)[100], (001)[010], and (010)[001], which are not available for (210) shocks.

Interesting observations can be made by considering specific shock strengths.P_{RH} values of magnitude 7, 2.14, and 1.24 GPa are considered. These values are chosen on the basis of previous experimental studies[4,5,7] and represent critical thresholds for RDX. P_{RH} = 7 GPa is the minimum experimental peak stress reported for decomposition in RDX.[7] Low stress flyer-plate impact experiments reported an abrupt change in the response of RDX for (111)[4] and (021)[6] shocks for 1.24 < P_{RH} < 2.14 GPa. Values of the resolved shear stress (τ_{RSS}) for all slip systems are shown in Figure 10 against the lowest values of τ_{PN} in the respective system, for (111) shocks with P_{RH} = 7, 2.14, and 1.24 GPa and for a (210) shock withP_{RH} = 7 GPa.

For a P_{RH} of 7 GPa it results that all seven slip systems with nonvanishing Schmid factors have $\tau_{RSS} > \tau_{PN}$ for (111) shocks. (210) shocks activate five slip systems. However, the sensitivity is higher for (210) shocks.[7] On the basis of this observation a lower number of slip systems results in hindered plasticity and the inability of the crystal to relax the applied stress. Thus the present study confirms the validity of the steric hindrance model pertaining to the decomposition of RDX. A recent computational study of compressive dynamic loading using a reactive force field also supports the validity of the steric hindrance model.[25] It should be noted that the RDX crystals undergo an $\alpha-\gamma$ phase transition at pressures above 4.5 GPa[26] for shock and between 2 and 4 GPa[27,28] under quasi-static loading conditions. In addition to the phase transition, the high strain rates and temperatures involved in a shock might result in more complicated deformation mechanisms compared to what can be inferred from quasi-static simulations.

For P_{RH} = 2.14 GPa in a (111) shock, at least five slip systems (with $m \neq 0$) remain active. If one considers P_{RH} = 1.24 GPa and the (111) shock, only the (010)[100] system is clearly activated. Thus the observed change in response of (111) oriented crystals can be attributed to the activation of a higher number of slip systems as the shock pressure increases. Also, for (111) shocks, the cross-slip of [100] screw dislocations will be inhibited at lower shock pressure and this might also play a role in controlling the deformation behavior.

In the case of (021) shocks (not shown), P_{RH} = 2.14 GPa activates the (001)[010] and (010)[001] slip systems. A shock of P_{RH} = 1.24 GPa will activate only the (001)[010] system. Thus the above conclusion that anisotropic response can be correlated with differential activation of slip systems remains unchanged for the (021) shocks.

Shocks normal to the (100) plane activate none of the slip systems considered in this work. It is possible that other deformation mechanisms[4,29] and/or other slip systems become active in order to accommodate the imposed deformation.

5. CONCLUSIONS

Atomistic simulations in conjunction with the Peierls–Nabarro model were used to study the mobility of dislocations in RDX. This study indicates that the (010)[100] slip system has the least resistance to dislocation motion. Screw dislocations of the [100] type on (021), (001), and (011) planes were found to have Peierls stress values within 10% of each other, supporting

dx.doi.org/10.1021/jp401368t | J. Phys. Chem. A 2013, 117, 5326–5334

the conjecture that cross-slip of screw segments with [100] orientation is possible. Critical stresses were found to be between $G_v/20$ and $G_v/10$ for the majority of the slip systems investigated. However, the number of independent slip systems is always lower than the minimum of five required for the accommodation of a general strain state; hence plasticity in RDX is hindered. The anisotropic sensitivity of RDX crystals shocked in (111) and (210) directions can be explained in terms of differential mobility on available slip systems, and this supports the validity of the steric hindrance model for this material. An explanation for the anomalous response at low shock pressures is also provided in terms of the activation of available slip systems.

AUTHOR INFORMATION

Notes

The authors declare no competing financial interest.

ACKNOWLEDGMENTS

N.M. and R.C.P. gratefully acknowledge the support from the Army Research Office through Grant W911NF-09-1-0330, program director Dr. Joseph Myers.

REFERENCES

(1) Field, J. E. Hot Spot Ignition Mechanisms for Explosives. *Acc. Chem. Res.* **1992**, *25*, 489−496, DOI: 10.1021/ar00023a002.

(2) Armstrong, R. W.; Ammon, H. L.; Elban, W. L.; Tsai, D. H. Investigation of Hot-Spot Characteristics in Energetic Crystals. *Thermochim. Acta* **2002**, *384*, 303−313, DOI: 10.1016/S0040-6031(01)00786-9.

(3) Dick, J. Anomalous Shock Initiation of Detonation in Pentaerythritol Tetranitrate Crystals. *J. Appl. Phys.* **1997**, *81*, 601−612, DOI: 10.1063/1.364201.

(4) Hooks, D. E.; Ramos, K. J.; Martinez, A. R. Elastic-Plastic Shock Wave Profiles in Oriented Single Crystals of Cyclotrimethylene Trinitramine (RDX) at 2.25 GPa. *J. Appl. Phys.* **2006**, *100*, 024908 DOI: 10.1063/1.2214639.

(5) Cawkwell, M. J.; Ramos, K. J.; Hooks, D. E.; Sewell, T. D. Homogeneous Dislocation Nucleation in Cyclotrimethylene Trinitramine under Shock Loading. *J. Appl. Phys.* **2010**, *107*, 063512 DOI: 10.1063/1.3305630.

(6) Ramos, K. J.; Hooks, D. E.; Sewell, T. D.; Cawkwell, M. J. Anomalous Hardening Under Shock Compression in (021)-Oriented Cyclotrimethylene Trinitramine Single Crystals. *J. Appl. Phys.* **2010**, *108*, 066105 DOI: 10.1063/1.3485807.

(7) Dang, N. C.; Dreger, Z. A.; Gupta, Y. M.; Hooks, D. E. Time-Resolved Spectroscopic Measurements of Shock-Wave Induced Decomposition in Cyclotrimethylene Trinitramine (RDX) Crystals: Anisotropic Response. *J. Phys. Chem. A* **2010**, *114*, 11560−11566, DOI: 10.1021/jp106892c.

(8) Connick, W.; May, F. G. J. Dislocation Etching of Cyclotrimethylene Trinitramine Crystals. *J. Cryst. Growth* **1969**, *5*, 65−69, DOI: 10.1016/0022-0248(69)90077-3.

(9) McDermott, I. T.; Phakey, P. P. A Method of Correlating Dislocations and Etch Pits: Application to Cyclotrimethylene Trinitramine. *J. Appl. Crystallogr.* **1971**, *4*, 479−481, DOI: 10.1107/S0021889871007490.

(10) Gallagher, H. G.; Halfpenny, P. J.; Miller, J. C.; Sherwood, J. N.; Tabor, D. Dislocation Slip Systems in Pentaerythritol Tetranitrate (PETN) and Cyclotrimethylene Trinitramine (RDX) [and Discussion]. *Philos. Trans. R. Soc. London, Ser. A* **1992**, *339*, 293−303, DOI: 10.1098/rsta.1992.0036.

(11) Halfpenny, P. J.; Roberts, K. J.; Sherwood, J. N. Dislocations in Energetic Materials. *J. Mater. Sci.* **1984**, *19*, 1629−1637, DOI: 10.1007/BF00563061.

(12) Ramos, K. J.; Hooks, D. E.; Bahr, D. F. Direct Observation of Plasticity and Quantitative Hardness Measurements in Single Crystal Cyclotrimethylene Trinitramine by Nanoindentation. *Philos. Mag.* **2009**, *89*, 2381−2402, DOI: 10.1080/14786430903120335.

(13) Munday, L.; Solares, S.; Chung, P. W. Generalized Stacking Fault Energy Surfaces in the Molecular Crystal RDX. *Philos. Mag.* **2012**, *92*, 37−41, DOI: 10.1080/14786435.2012.685191.

(14) Rice, J. R. Dislocation Nucleation from a Crack Tip: An Analysis based on the Peierls Concept. *J. Mech. Phys. Solids* **1992**, *40*, 239−271, DOI: 10.1016/S0022-5096(05)80012-2.

(15) Elban, W. L.; Armstrong, R. W.; Yoo, K. C.; Rosemeier, R. G.; Yee, R. Y. X-ray Reflection Topographic Study of Growth Defect and Microindentation Strain fields in an RDX Explosive Crystal. *J. Mater. Sci.* **1989**, *24*, 1273−1280, DOI: 10.1007/BF02397058.

(16) Smith, G. D.; Bharadwaj, R. K. Quantum Chemistry Based Force Field for Simulations of HMX. *J. Phys. Chem. B* **1999**, *103*, 3570−3575, DOI: 10.1021/jp984599p.

(17) Sorescu, D. C.; Rice, B. M.; Thompson, D. L. Intermolecular Potential for the Hexahydro-1,3,5-trinitro-1,3,5-s-triazine Crystal (RDX): A Crystal Packing, Monte Carlo, and Molecular Dynamics Study. *J. Phys. Chem. B* **1997**, *101*, 798−808, DOI: 10.1021/jp9624865.

(18) Stroh, A. N. Dislocations and Cracks in Anisotropic Elasticity. *Philos. Mag.* **1958**, *7*, 625−646, DOI: 10.1080/14786435808565804.

(19) Choi, C. S.; Prince, E. The Crystal Structure of Cyclotrimethylenetrinitramine. *Acta Crystallogr., Sect. B: Struct. Sci.* **1972**, *28*, 2857−2862, DOI: 10.1107/S0567740872007046.

(20) Plimpton, S. J. Fast Parallel Algorithms for Short-Range Molecular Dynamics. *J. Comput. Phys.* **1995**, *117*, 1−19, DOI: 10.1006/jcph.1995.1039. http://lammps.sandia.gov.

(21) Hull, D.; Bacon, D. J. *Introduction to Dislocations*; Butterworth-Heinemann: Oxford, U.K., 2001; pp 15, 65−69.

(22) Hearmon, R. The Elastic Constants of Anisotropic Materials II. *Adv. Phys.* **1956**, *5*, 323−382, DOI: 10.1080/00018732.1956.tADP0323.

(23) Kocks, U. F. Independent Slip Systems in Crystals. *Philos. Mag.* **1964**, *10*, 187−193, DOI: 10.1080/14786436408225657.

(24) Groves, G.; Kelly, A. Independent Slip Systems in Crystals. *Philos. Mag.* **1963**, *8*, 877−887, DOI: 10.1080/14786436308213843.

(25) An, Q.; Zybin, S.; Sergey, V.; Hyungjun, K.; Goddard, W. A., III. Anisotropic Shock Sensitivity of Cyclotrimethylene Trinitramine (RDX) from Compress-and-Shear Reactive Dynamics. *J. Phys. Chem. C* **2012**, *116*, 10198−10206, DOI: 10.1021/jp300711m.

(26) Patterson, J. E.; Dreger, Z. A.; Gupta, Y. M. Shock Wave-Induced Phase Transition in RDX Single Crystals. *J. Phys. Chem. B* **2007**, *111*, 10897−10904, DOI: 10.1021/jp079502q.

(27) Dreger, Z. A.; Gupta, Y. M. Phase Diagram of Hexahydro-1,3,5-trinitro-1,3,5-triazine Crystals at High Pressures and Temperatures. *J. Phys. Chem. A* **2010**, *114*, 8099−8105, DOI: 10.1021/jp105226s.

(28) Munday, L. B.; Chung, P. W.; Rice, B. M.; Solares, S. D. Simulations of High-Pressure Phases in RDX. *J. Phys. Chem. B* **2011**, *115*, 4378−4386, DOI: 10.1021/jp112042a.

(29) Cawkwell, M.; Sewell, T.; Zheng, L.; Thompson, D. Shock-Induced Shear Bands in an Energetic Molecular Crystal: Application of Shock-Front Absorbing Boundary Conditions to Molecular Dynamics Simulations. *Phys. Rev. B* **2008**, *78*, 014107 DOI: 10.1103/PhysRevB.78.014107.